



5-2011

Targeted Synthesis and Characterization of Isolated Zirconium (IV) Centers in a Silicate Building Block Matrix

Katherine P. Sharp
kpsharp9@gmail.com

Follow this and additional works at: http://trace.tennessee.edu/utk_chanhonoproj

 Part of the [Inorganic Chemistry Commons](#)

Recommended Citation

Sharp, Katherine P., "Targeted Synthesis and Characterization of Isolated Zirconium (IV) Centers in a Silicate Building Block Matrix" (2011). *University of Tennessee Honors Thesis Projects*.
http://trace.tennessee.edu/utk_chanhonoproj/1449

This Dissertation/Thesis is brought to you for free and open access by the University of Tennessee Honors Program at Trace: Tennessee Research and Creative Exchange. It has been accepted for inclusion in University of Tennessee Honors Thesis Projects by an authorized administrator of Trace: Tennessee Research and Creative Exchange. For more information, please contact trace@utk.edu.

Targeted Synthesis and Characterization of Isolated Zirconium (IV) Centers in a Silicate Building Block Matrix

A report of the research conducted by Katherine P. Sharp in the laboratory of Dr. C.E. Barnes under the mentorship of Mr. M.E. Peretich from Fall 2009 to Spring 2011,

Submitted in partial fulfillment of the requirements of a
Bachelor of Science Degree in Chemistry with Honors,

Presented to my faculty committee,
Drs. R.J. Hinde, J. Kovac, and C. E. Barnes (advisor)

April 29, 2011

Table of Contents

Introduction	4
Materials and Methods.....	10
Materials	10
Synthesis of 4-connected “embedded” zirconium centers in Si ₈ O ₂₀ -based building block matrices	11
Characterization.....	11
Gravimetric Analysis	12
Surface area and Porosity measurements.....	12
Infrared (IR) Spectroscopy	12
Extended X-Ray Absorption Fine Structure (EXAFS) Spectroscopy.....	13
Results and Discussion	14
X-Ray Absorption Study	17
Pyridine binding to 4C-Zr: An IR Study.....	27
Surface Area versus Stoichiometric Dosing Ratios Study	29
Conclusions and Future Work.....	33
References	35

Table of Figures

Figure 1: Isomorphous substitution of silicon, Si, with a metal, M	5
Figure 2: Complementary functional groups on linking agents and building block	6
Figure 3: Trimethyltin functionalized cubic silicate building block, $\text{Si}_8\text{O}_{12}(\text{OSnMe}_3)_8$	7
Figure 4: Cross-linking metathesis reaction between trimethyltin functionalized silicate building block ($\text{Si}_8\text{O}_{12}(\text{OSnMe}_3)_8$) and metal chloride (MCl_n)	8
Figure 5: Growth model for isolated zirconium centers in a silicate matrix.....	9
Figure 6: ^1H NMR (250 MHz) of volatiles containing Me_3SnCl by-product	16
Figure 7: Structure of "embedded" zirconium center	16
Figure 8: E-space plot first dose ZrCl_4	18
Figure 9: Theoretical model with important bond lengths and angles highlighted	19
Figure 10: Non-EXAFS feature due to double electron transition	21
Figure 11: R-space plot first dose ZrCl_4	22
Figure 12: k-space plot first dose ZrCl_4	23
Figure 13: R-space plot second dose SiCl_4	25
Figure 14: k-space plot second dose SiCl_4	25
Figure 15: R-space plot second dose SiCl_4py_2	26
Figure 16: k-space plot second dose SiCl_4py_2	26
Figure 17: Excerpt of IR Spectrum showing C-C ring vibrations indicative of pyridine bound to Lewis acidic Zr sites.....	27
Figure 18: Potential acidic sites in the silicate matrices	28
Figure 19: BET surface area versus stoichiometric ratio for a series of first dose Si materials	30
Figure 20: Total pore volume versus stoichiometric ratio for a series of first dose Si materials	30
Figure 21: Comparison of adsorption and desorption isotherms for high and low stoichiometric ratios ..	31
Figure 22: Comparison of BJH plots for high and low stoichiometric ratios.....	32
Figure 23: BET surface area versus stoichiometric ratio for a series of first and second dose Si, Ti, and Zr materials	33

Introduction

Catalysts are important materials that are extensively studied for their use in industrial chemistry. In a catalytic reaction, the rate of the reaction is increased by the addition of small amount of a material, the catalyst, which is not consumed during the reaction process. The characteristics of effective catalytic materials are high selectivity, activity, and stability. A catalyst should assist in the production of only one desired product, it should be able to quickly process substrates to produce this desired product, and remain unchanged throughout the process. A catalyst can either be homogeneous, functioning in the same phase as the reactants, or it can be heterogeneous and catalyze a reaction from a separate phase than the reactants. Homogeneous catalysts have been extensively studied and are thus better defined than heterogeneous catalysts. Since homogeneous catalysts work within the same phase as the reactants it can be difficult to separate the reaction product from the catalytic material. Furthermore, from an industrial standpoint, the difficult separation of homogeneous catalysts from the reaction product is neither time nor cost effective. This is one reason for the recent interest in developing better ways to synthesize and characterize heterogeneous catalysts for use in industry.

In the field of catalysis science the synthesis of single-site heterogeneous catalysts which possess high site densities and surface areas is of fundamental importance but remains quite challenging experimentally. These challenges arise from the preparation methods for traditional heterogeneous catalysts such as mixed metal oxides, templated sol-gels, and zeolites.¹ The main challenge of these methodologies is the ability to synthesize materials with diverse functionality while maintaining structure at many different scales and stages throughout the synthesis. Microporous, crystalline aluminosilicate materials, known as zeolites, are one example of traditional heterogeneous catalysts that are of great interest. Zeolites with isomorphous metal substitution are

highly active catalysts that are widely used in industry. Figure 1 illustrates the active sites of substitution. Isomorphous substitution of elements such as Ga, Ce, Be, B, Fe, Cr, P, and Mg for Si or Al in zeolite frameworks have been researched.²

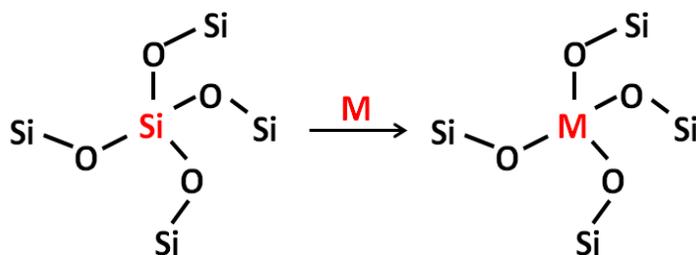


Figure 1: Isomorphous substitution of silicon, Si, with a metal, M

Isomorphous substitutions are thought to result in increased rigidity of the framework which ensures the surface area and pore size distribution of the catalyst remains unchanged throughout the reaction.³

Despite these positive aspects, challenges still remain in the methodologies used to prepare heterogeneous catalysts from zeolites. The isomorphous substitution of the metal into the zeolite framework is not thought to be a highly controlled process and so the resulting catalyst may not contain a single type of active site responsible for catalytic activity. Similarly, the methods used in preparing mixed metal oxides or using sol-gel template materials to prepare heterogeneous catalysts can exhibit the same site homogeneity problem encountered with zeolite materials as well as problems with stability and accessibility. There may be multiple sites in these materials that contribute to the catalysis, leading to production of multiple products and thus to low selectivity. Zeolites have proven to be excellent catalysts in many respects, but are limited primarily to microporous solids. A different methodology for preparing heterogeneous catalysts, which focuses on control of the sites that are developed as well as surface area and porosity, can improve their efficiency by addressing problems with selectivity and activity, as well as maintaining stability.

In an effort to address the challenges briefly described above, a method is being developed for the targeted preparation of high surface area silicate matrices that contain a single type of

isolated metal center. A single site catalyst is naturally expected to be more selective than a catalyst with multiple active sites. Another goal of this methodology is to produce a support matrix with a high density of sites while maintaining site isolation. Since catalysis takes place on the surface of the catalysts, production of a high surface area, porous, matrix is necessary to produce high site density materials, which should increase the activity of the potentially catalytic material by increasing mass transfer rates for the substrates. Finally, the active site must remain in place on the surface of the support matrix during the catalytic reaction. The metal must not be leached from the support matrix during the reaction process.

To achieve the goals outlined above, three things have been identified as necessary components for this developing methodology. The first component is a rigid building block that will be the main structure directing agent. Secondly, two types of linking agents are required. The first type of linking agent “inserts” the metal centers that will become the catalytic sites in the matrix and the second produces additional chemically robust linkages between the molecular building blocks to help stabilize the matrix. The last component required to achieve these specific goals is a linking reaction between the rigid building block and the two types of linking reagents. This linking reaction must occur between complementary functional groups on the building block and linking agents to prevent self-condensation of the functional groups. An example of this complementary linking reaction is diagramed in Figure 2.

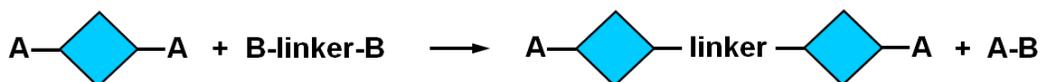


Figure 2: Complementary functional groups on linking agents and building block

In the methodology described in this report, a metal center is introduced into the matrices through a metal chloride linking agent reacted with a rigid, trimethyltin functionalized cubic silicate

building block, $\text{Si}_8\text{O}_{12}(\text{OSnMe}_3)_8$. The silicate building block possesses a cubic structure with a silicon on each of the corners connected to three bridging oxygens and one $-\text{OSnMe}_3$ group as seen in Figure 3.⁴⁻⁶

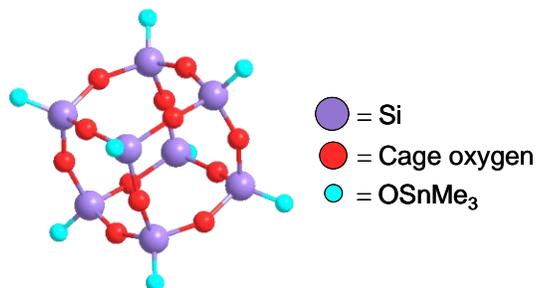


Figure 3: Trimethyltin functionalized cubic silicate building block, $\text{Si}_8\text{O}_{12}(\text{OSnMe}_3)_8$

The bond formation between the silicate building blocks involves the metathesis reaction of a Me_3Sn group, bound to the oxygen on the corner of the building block, with a chloride ligand of a high valent metal or main group element as seen in Figure 4. The complementary nature of the functional groups on the silicate building block (Me_3Sn) and metal (Cl) ensures atomic dispersion throughout the matrix because self-condensation cannot occur. The reaction of the building block with the linking agent is irreversible. Furthermore, the corners of the silicate building block react largely independently of one another, which leads to random substitution patterns around the corners of the cubic building blocks. This irreversibility and indiscriminate method of linking building blocks with the linking agents causes the resulting matrix to be amorphous. This amorphous matrix is also expected to contain void volumes creating a porous material.

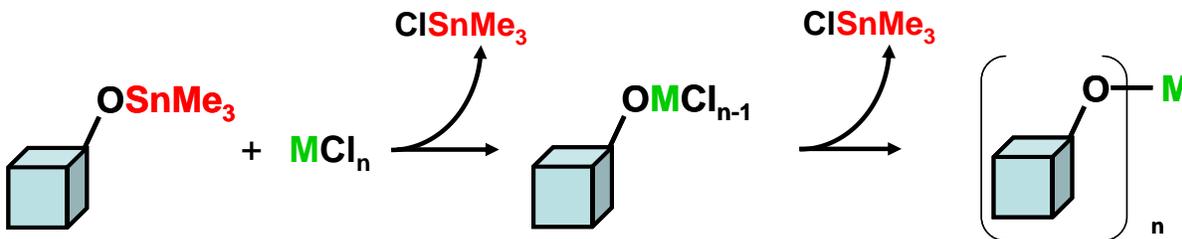


Figure 4: Cross-linking metathesis reaction between trimethyltin functionalized silicate building block ($\text{Si}_8\text{O}_{12}(\text{OSnMe}_3)_8$) and metal chloride (MCl_n)

The exchange process between the Me_3Sn groups on the building blocks and the chloride ligand of the linking agent continues until all of the chloride ligands on the metal are consumed or a Me_3Sn group becomes inaccessible to a chloride ligand. The overall “connectivity” achieved by the metal is defined by the number of metal-oxygen-silicon bonds formed during the reaction. If, after the addition of a limiting amount of the metal chloride in the first dosing step all of the chloride ligands react, then all the metal centers will have the same connectivity and be identical to one another.

During the first dosing step, the nanometer-sized silicate building blocks are cross-linked together into small, second generation oligomer building blocks. By carefully choosing the size of the initial dose of the metal chloride, the growth should transform from the linking together of silicate building blocks to linking together small oligomer building blocks. The silicate building block matrix is then built around the metal center established in the first dose of metal chloride by the controlled addition of a second cross-linking agent such as a silyl chloride. A second dose of cross linking reagent will then link together these new small oligomer building blocks to form a porous matrix. This model for the growth of the matrix around the active site is diagramed in Figure 5. This method is distinct from the method of isomorphous substitution which requires insertion of the metal into a pre-existing matrix.

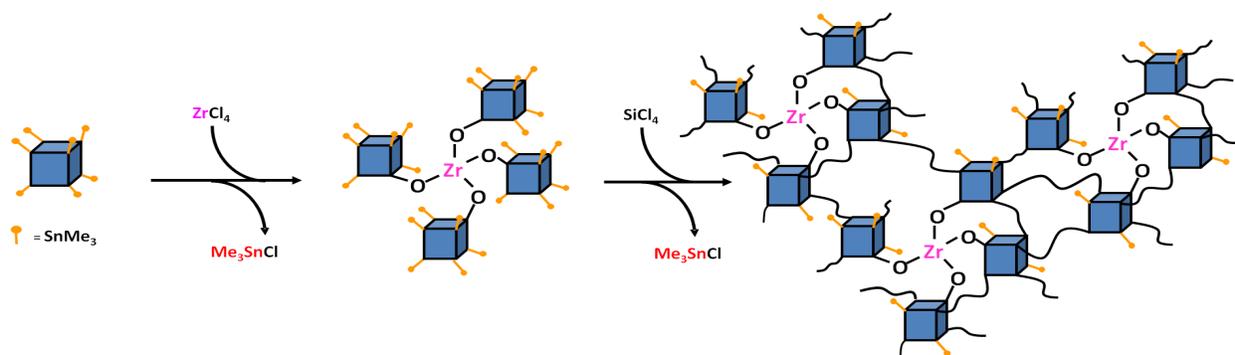


Figure 5: Growth model for isolated zirconium centers in a silicate matrix

Based on the methodology described above, a strategy of sequential additions and careful adjustment of parameters such as the reaction stoichiometry has been developed to tailor several properties of the matrices. Some strengths of this methodology are that a single type of metal center is achieved through the simple adjustment of the stoichiometric ratios of the reactants, the high surface area support is grown around existing active sites, which prevents the aggregation of active sites.⁷

The work described here focuses on incorporating zirconium into the synthetic strategy described above. Dongare has described the successful isomorphous substitution of Zr^{4+} for Si^{4+} in a ZSM-5 zeolite framework.⁸ Zr-ZSM-5 was concluded to be catalytically active in the hydroxylation of benzene.⁸ There have also been reports of the catalytic activity for Zr-MCM-41 in the oxidation of cyclohexane, cyclohexene, and vinyl-cyclohexene.⁹ The catalytic activity of the zirconium centers in the matrices prepared via the methodology reported here will be investigated in selective oxidation reactions such as the epoxidation of olefins.

Gravimetric analysis, infrared spectroscopy (IR), XANES, and extended x-ray absorption fine structure (EXAFS) spectroscopy were used to characterize the resulting zirconium centers in these building block matrices. This characterization will highlight the ability of this methodology to address the problems currently faced by those attempting to prepare well defined, heterogeneous

catalysts. The method of sequential additions and proper stoichiometric ratios ensures the presence of a single type of active site within a high surface area matrix, which will hopefully address the challenges of selectivity and accessibility. Future work with these matrices will include the testing of their catalytic activity as outlined above in addition to investigating new methods of passivating unreacted chlorides present after the second dosing step, and calcination.

Materials and Methods

Materials

The reactions described in this paper involve air-sensitive materials, which require performing the reactions in high vacuum environments, and storing reagents in a nitrogen atmosphere glove box. The solvents used in these reactions, tetrahydrofuran and toluene, were dried over Na/K alloy and distilled. Zirconium (IV) chloride ($ZrCl_4$, 99.5%, white powder) and pyridine (99%) were obtained from Aldrich and used as received. Tetrachlorosilane ($SiCl_4 > 99.5\%$) was obtained from Fisher Scientific. Silicon tetrachloride bis-pyridine ($SiCl_4py_2$) was produced according to the literature and stored and added to reaction vessels in a nitrogen atmosphere glove box.¹⁰ $SiCl_4$ and pyridine were stored under vacuum in Schlenk vessels with Teflon stopcocks. All reaction flasks were treated with chlorotrimethylsilane and triethyl amine before using them for the reactions. In addition, the reaction flasks were flame dried to remove any trace amount of water remaining in the flasks. The reagents and solvents used were vapor transferred into the reaction flasks, and the amount delivered determined gravimetrically.

Synthesis of 4-connected “embedded” zirconium centers in Si_8O_{20} -based building block matrices

2.00 g (1.08 mmol) dehydrated $(\text{Me}_3\text{SnO})_8\text{Si}_8\text{O}_{12}$ and 0.126 g (0.54 mmol) ZrCl_4 were added together to a Schlenk vessel in a N_2 atmosphere glove box. The reaction vessel was removed from the glove box and 25 mL THF was vapor transferred into the reaction vessel. The reaction was stirred vigorously under static vacuum for 24h at 60°C . During the reaction process, no gel or precipitate was seen to form. After this time the solvent and byproduct, Me_3SnCl , were removed under vacuum at 100°C for an additional 24h.

After the initial dosing reaction, which integrated zirconium into the silicon-based building block matrix, 25 mL of toluene were vapor transferred to the reaction vessel followed by 0.55 g SiCl_4 (3.24 mmol). The second linking agent was vapor transferred into the Schlenk vessel and after its addition the solution was allowed to stir under static vacuum for 24h at 80°C . Silicon tetrachloride bis-pyridine, SiCl_4py_2 , can also be used as a second linking agent at the same molar ratio to $\text{Si}_8\text{O}_{12}(\text{OSnMe}_3)_8$. During the reaction process a gelatinous product formed prior to solvent removal. After the removal of volatiles and drying under vacuum at 100°C , an off-white solid product was obtained. The product was characterized without any further purification.

Characterization

Gravimetric analysis, nitrogen adsorption and desorption isotherms, infrared spectroscopy, and extended x-ray absorption fine structure (EXAFS) spectroscopy were the methods used to characterize these tailored silicate matrices containing zirconium centers.

Gravimetric Analysis

Following the first cross-linking reaction, the product is separated from the solvent and the volatile byproduct Me_3SnCl under vacuum. In each cross-linking reaction there is the potential for varying degrees of connectivity based on the number of chlorides that reacted from ZrCl_4 . The connectivity of the zirconium center is revealed by the amount of Me_3SnCl produced during the cross-linking reaction. Gravimetric data, the weight change after each cross-linking reaction, determines the average connectivity of each zirconium center in the silicate matrix. Maximum connectivity is achieved when all of the chlorides on ZrCl_4 have reacted to form Me_3SnCl . In the case where maximum connectivity is attained, all of the zirconium centers will be connected identically throughout the matrix.

Surface area and Porosity measurements

The surface area and pore volumes of the matrices were determined using data collected with a Quanta Chrome Corp. Nova 1000 High Speed Surface Area and Pore Size Analyzer. The surface area was determined using adsorption data by the method proposed by Brunauer, Emmett, and Teller (BET) in the relative pressure range from 0.05 to 0.35.¹¹ The pore size distribution was computed using the method proposed by Barrett, Joyner, and Halenda (BJH).¹²

Infrared (IR) Spectroscopy

Infrared samples were prepared and spectra were collected using a Thermo Nicolet IR100 in a MBraun LabMaster 130 dry box (N_2). The IR spectra collected for these zirconium silicate matrices were used to examine the pyridine adsorption and determine the acidity of the zirconium centers in the silicate matrix. To produce these spectra a KBr pellet without the sample was first prepared and

the data collected as a background spectrum. Then another pellet was prepared that contains a sample of the product from a second dosing reaction with SiCl_4py_2 . Three absorptions in the range of 1400 cm^{-1} to 1700 cm^{-1} assigned to C-C ring vibrations were used to identify the acidic nature of the zirconium centers in the silicate matrix.¹³

Extended X-Ray Absorption Fine Structure (EXAFS) Spectroscopy

EXAFS samples were prepared under dry nitrogen atmosphere and placed into copper sample cells with Kapton® (Chemplex 442) windows sealed with two-sided transparent tape. Zirconium K-edge (17.998 keV) data was collected in both transmittance and fluorescence mode at the National Synchrotron Light Source (NSLS) on beam line X18B (unfocussed beam) operated at 2.8 GeV with a current of 300-100 mA. Spectra were collected at room temperature. The incident beam was detuned 20% to suppress harmonics. Samples were mounted 45° to the beam in order to collect transmission and fluorescence spectra simultaneously. The intensity of the incident beam was measured with an 18 cm 70:30 N_2 : Ar-filled ion chamber detector (I_0). Transmitted x-rays were detected in a 30 cm 90:10 Ar: Kr-filled ion chamber (I_t). The fluorescence signal from the sample was recorded with a Canberra PIPS detector (I_{fluor}). Scans were calibrated against a Zr foil (17.998 eV). Two scans were collected for each sample with beam dimensions on sample: 11 mm x 1.5 mm (w x h). Data collection parameters are summarized in Table I.

Table I: Collection Parameters

Regions	Resolution	Integration Time
-150 eV to -15 eV	5 eV	1
-15 eV to 75 eV	1.3 eV	2
75 eV to 12k	0.05k	3
12k to 18k	0.05k	4

Absorption data were analyzed with the IFEFFIT data analysis software suite (Athena & Artemis).^{14,15} The Athena program was used to merge several scans for each sample into a single file, in addition to extracting EXAFS from the smooth absorption edge background. The EXAFS data was modeled using the program FEFF, included in the Artemis program.¹⁶ Theoretical phase and amplified EXAFS functions were obtained from FEFF 6 based on a proposed structural model. These were then used in a least squares fitting to $\chi(k)$ data. An estimate of the amplitude reduction factor was determined to be 0.928 using FEFF 8 and was set to that value for the modeling.¹⁷ Initial fits were made by setting the coordination number of zirconium to expected values determined from gravimetric analysis and varying the remaining parameters. The coordination number of zirconium was then refined.

Results and Discussion

The general synthetic methodology described here for the synthesis of isolated transition metal centers in high surface area silicate matrices involves an initial dosing step where a metal chloride complex, in this case zirconium (IV) chloride, reacts with a trimethyltin functionalized, spherosilicate building block, $\text{Si}_8\text{O}_{12}(\text{OSnMe}_3)_8$.^{7,18} The number of chloride ligands of ZrCl_4 that react can be controlled by varying the stoichiometric ratio of ZrCl_4 to $\text{Si}_8\text{O}_{12}(\text{OSnMe}_3)_8$. Gravimetric analysis indicates that at a stoichiometric ratio of 0.5 ZrCl_4 : 1.0 $\text{Si}_8\text{O}_{12}(\text{OSnMe}_3)_8$ all of the chloride ligands of ZrCl_4 react with the trimethyltin groups of $\text{Si}_8\text{O}_{12}(\text{OSnMe}_3)_8$ resulting in the formation of four Zr-O-Si linkages and four equivalents of the volatile by-product Me_3SnCl .

Empirically, we determined that the maximum stoichiometric ratio that would still produce the desired four Zr-O-Si linkages, and leads to an embedded zirconium center, is two building blocks

for every zirconium. The possibility of not achieving zirconium centers with maximum connectivity can arise when the growth model described previously is altered. If too much $ZrCl_4$ is used initially, small oligomers are cross-linked to produce larger oligomers prior to reaction with $ZrCl_4$, and the matrix will become rigid. The remaining $SnMe_3$ groups will be spatially isolated making them unable to react with the chloride ligands of $ZrCl_4$.

The connectivity achieved in the reaction of a limiting amount of $ZrCl_4$ with the silicate building block can be determined from the production of the Me_3SnCl by-product. The presence of Me_3SnCl as the only by-product was verified by 1H NMR, which confirms the notion that zirconium formed linkages with the silicate building block. The 1H NMR spectrum was collected on a 250 MHz NMR using C_6D_6 as the solvent. The spectrum shown in Figure 6 reveals the presence of singlet peak due to the methyl protons of Me_3SnCl in THF around 0.46 ppm and characteristic tin satellites. The satellites appear as doublets due to the isotopes, Sn-117 and Sn-119. The coupling constant $J(^{119}Sn-^1H)$ for the outer peaks in the doublet was calculated at 62 Hz and the coupling constant $J(^{117}Sn-^1H)$ for the inner peaks in the doublet was found to be 60 Hz.

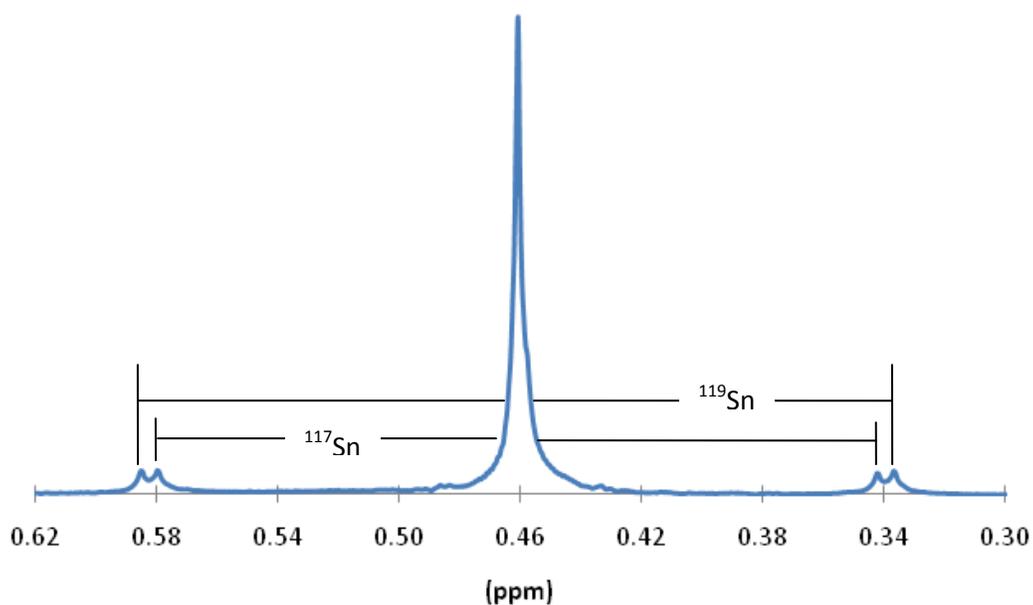


Figure 6: ^1H NMR (250 MHz) of volatiles containing Me_3SnCl by-product

Gravimetric determination of the connectivity of zirconium to silicate building blocks, for a $0.5 \text{ ZrCl}_4 : 1.0 \text{ Si}_8\text{O}_{20}(\text{OSnMe}_3)_8$ stoichiometric ratio, gives 4.0 ± 0.1 connected zirconium centers. This determination of the connectivity highlights the conclusion that all four zirconium chloride ligands reacted with trimethyltin groups on the silicate building blocks. The gravimetric data indicate that there is a single type of zirconium site present in the matrix that contains four Zr-O-Si linkages. When each zirconium center is bound to four silicate building blocks these centers are referred to as "embedded" or framework metal centers (Figure 7).

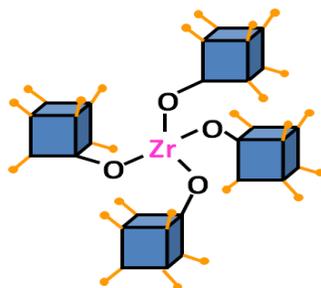


Figure 7: Structure of "embedded" zirconium center

BET analysis performed on the product after the first cross-linking reaction revealed the matrix to have no surface area. This indicates that the linking together of these nanometer sized silicate building blocks around the zirconium center produces small oligomers with negligible surface area as seen in the diagram of the growth model shown earlier (Figure 5).

A second dose of an additional cross-linking reagent, e.g. silicon tetrachloride or silicon tetrachloride bis-pyridine, links together these small oligomers resulting in the formation of a high surface area silicate support containing embedded zirconium centers. Unlike in the method of isomorphous metal substitution, in this synthetic methodology the embedded metal center is not altered as the high surface area silicate matrix is formed.

X-Ray Absorption Study

X-ray absorption spectroscopy (XAS) was employed as a characterization tool to investigate the immediate environment (out to $\sim 6 \text{ \AA}$) from the absorbing element, zirconium, in these silicate matrices. X-ray absorption results when an atom absorbs a photon, which excites a core electron into higher unoccupied electron orbitals. The hole left by the core electron is filled by an electron from a higher energy orbital, producing fluorescence. With zirconium as the absorbing atom, the ejected electron is a K-shell electron and the hole will be filled with either an L- or M-electron. XAS can be further divided into two specific types of analysis: X-ray absorption near edge structure (XANES) and extended X-ray absorption fine structure (EXAFS) analyses. A typical XAS spectrum for the zirconium samples is shown in Figure 8. The XANES region may be divided and analyzed in three regions, the pre-edge, position of the edge at E_0 , and top of the edge.

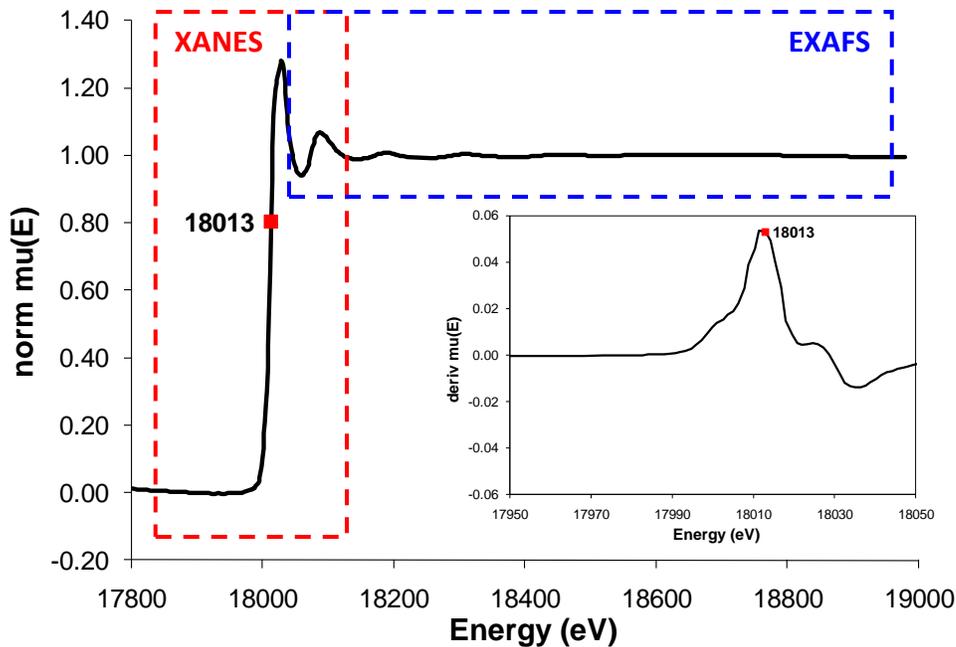


Figure 8: E-space plot first dose $ZrCl_4$

Pre-edge features are typically seen for metals in a tetrahedral environment, such as titanium, which results from dipole-allowed transitions between two bound states. Pre-edge features ($1s$ to $4d$ transition) would be expected for tetrahedral geometries around zirconium in these silicate matrices. Lack of a pre-edge can be indicative of octahedral geometry for a metal center. In the samples described here, a pre-edge feature is not observed in the XANES due to the increasing excitation energy and decreasing separation between $4d$ and $5p$ states of the second row transition metals, which causes this feature not to be resolved from the main ionization edge.¹⁹

The position of the absorption edge, E_0 , is defined as the point of inflection of the absorption edge and can be determined by finding the maximum of the derivative as seen in the insert in Figure 8. The value of E_0 will reveal information about the oxidation state of zirconium. In these silicate matrices an oxidation state of IV is expected for zirconium, and atoms of higher oxidation states with fewer electrons than protons should have absorption energies above that of the neutral atom. In the XANES analysis the K edge appears at an E_0 of 18013 eV, as defined by the inflection point in the edge. For

first and second dose samples the E_0 values range from approximately 14 to 15 eV above the E_0 for metallic zirconium (17998 eV). Each increase in oxidation state results in a 3 to 4 eV increase in the E_0 . Thus, the E_0 values for these samples are consistent with an oxidation state of IV for zirconium in these silicate matrices.

EXAFS is one of the few techniques that can probe the immediate environment of the zirconium centers in these amorphous silicate matrices. EXAFS analysis was used to verify the “embedded” nature of the zirconium centers by determining the first coordination sphere, atoms that are directly bound to Zr, and the second coordination sphere, atoms that are bound to the first coordination sphere atoms. In the EXAFS region of the XAS spectrum, the fine structure is extracted from the smooth absorption edge background and is displayed as $\chi(k)$ in reciprocal space (k-space) plots. The k-space data is then Fourier transformed and displayed as R-space plots. The data were fit to a theoretical model assuming a connectivity of four as supported by gravimetric analysis. The theoretical model, highlighting the bond lengths set for Zr-O and angles set for Zr-O-Si, can be seen in Figure 9.

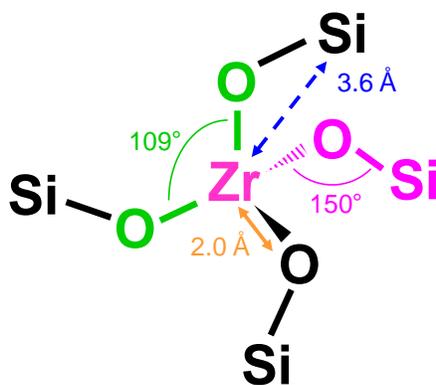


Figure 9: Theoretical model with important bond lengths and angles highlighted

Quantitative information is derived from a least squares fitting of the $\chi(k)$ data to the EXAFS equation, which is defined as the sum of all of the scattering paths as seen in Equation 1.

$$\chi(k) = \sum_i \chi_i(k) \quad \text{Eqn. 1}$$

Each scattering path is defined by Equation 2,

$$\chi_i(k) = \frac{(N_i S_0^2) F_{\text{eff}_i}(k)}{k R_i^2} \sin[2k R_i + \varphi(k)] e^{-2\sigma_i^2 k^2} e^{\frac{-2R_i}{\lambda(k)}} \quad \text{Eqn. 2}$$

where N_i is the coordination number of the i^{th} shell, S_0^2 is the amplitude reduction factor (also referred to as passive electron reduction factor), $F_{\text{eff}}(k)$ is effective scattering amplitude, $\varphi_i(k)$ is the effective scattering phase shift, σ_i^2 is the mean-square displacement of the bond length between the absorber atom and the coordination atoms in a shell (also referred to as Debye-Waller factor), and $\lambda(k)$ is the mean free path of the photoelectron.

The parameters tabulated for first and second dose samples of these zirconium matrices include R , σ^2 , E_0 , and CN. The bond distance between the absorbing atom, Zr, and the backscatterer in the first coordination sphere, O, or the separation distance between Zr and the backscatterer in the second coordination sphere, Si, are represented by parameters R_0 and R_{Si} . These values are compared to accepted literature values for these distances in comparable matrices. The value of σ^2 is a typical Debye-Waller factor and acceptable fits maintain values of σ^2 between 0.003 to 0.020 \AA^2 . The parameter E_0 is a value for the correction of the edge position and acceptable absolute values for this parameter are less than 10 eV. Finally, the coordination number, CN, is determined from the modeling of the EXAFS data to determine the number of backscattering atoms in a shell around the absorbing atom. This value should support the connectivity of the metal center determined by gravimetric analysis.

The k-range chosen to fit the EXAFS data with a theoretical model would ideally be the widest possible range because more data increases the resolution for the R-space plot. Prior to finalizing the k-range used for modeling the experimental data a non-EXAFS feature had to be

removed at $\sim 7.7 \text{ \AA}^{-1}$, which has been attributed to a double electron transition (circled in Figure 10).^{20,21} For the first dose sample the data in the range of 7.45 to 8.00 \AA^{-1} in the k-space plot was excluded from the fitting process, a more minor extraction than the reference range of 7.0 to 8.3 \AA^{-1} excluded by Mountjoy et al.²⁰

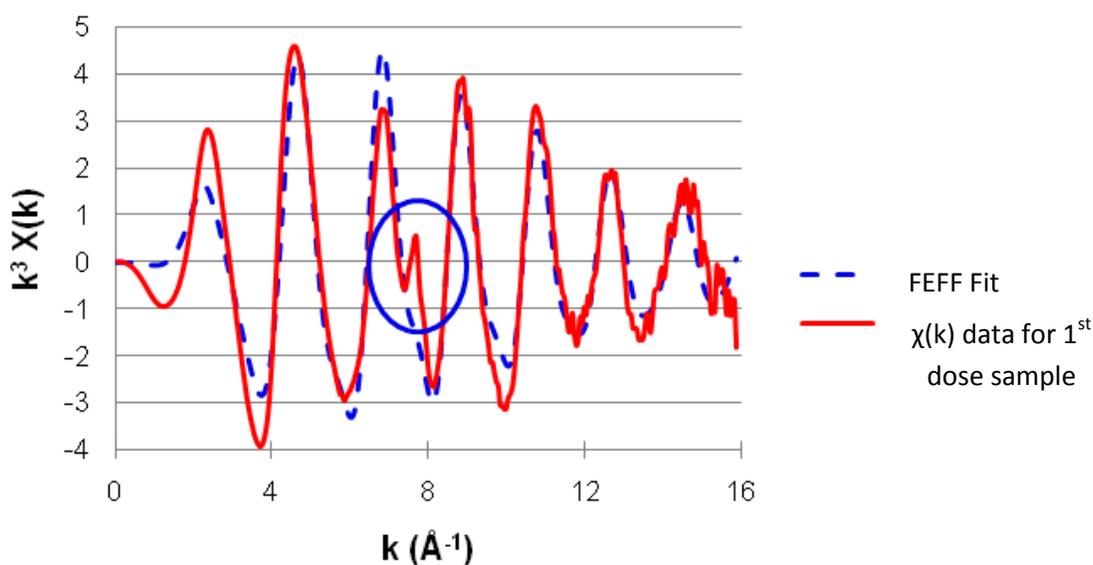


Figure 10: Non-EXAFS feature due to double electron transition

Based on gravimetric analysis a structural model containing an embedded zirconium center with four Zr-O-Si bonds and a tetrahedral geometry was chosen to model the data as seen in Figure 9. The FEFF 8 program was employed to predict the amplitude reduction factor (0.928) to be used in the modeling of the EXAFS data. Two paths, from zirconium to oxygen and zirconium to silicon, were the only paths considered in the modeling of the EXAFS data. The experimental k-space data was modeled against the theoretical data from the structural model at two possible k-ranges for the first dose sample, 4.1-15.1 \AA^{-1} and 5.2-15.1 \AA^{-1} . The resulting fits for these two k-ranges did not vary significantly in final refined fit parameters or the R-space plots produced from fitting to the structural model and so results from the larger k-range are reported in Table II. The structural parameters, R and k-space plots for the $\text{Zr}(\text{OSi})_4$ structural model can be seen in Table II, Figure 11,

and Figure 12. The main features of the R-space plot are the peak at 1.6 Å corresponding to the Zr-O bond and the peak at 3.1 Å corresponding to the path between Zr and Si. The distances seen in the R-space plot correspond to unphase corrected atom separations for Zr-O and Zr--Si, whereas the actual quantitative results of the fitting are really consistent with values from the literature.²²

Table II: Structural Parameters obtained from fits to first dose sample EXAFS data^a

	1 st dose	
	Zr-O (Lit.) ²²	Zr-Si (Lit.) ²²
R (Å)	2.002 (2.05)	3.62 (3.60)
σ^2 (Å) ²	0.0037	0.0074
E ₀ (eV)	-9.1 ± 1.4	E ₀ (O)
CN	3.8 ± 0.2	CN (O)

^a Additional fitting parameters as follows: amplitude reduction factor (S_0^2) 0.928. Fit figures of merit: 1st dose: FT k region: 4.1-15.1 Å⁻¹; X² 1367; reduced X² 71; R-factor 0.038. Non-EXAFS feature removal k region: 7.45-8.00 Å⁻¹.

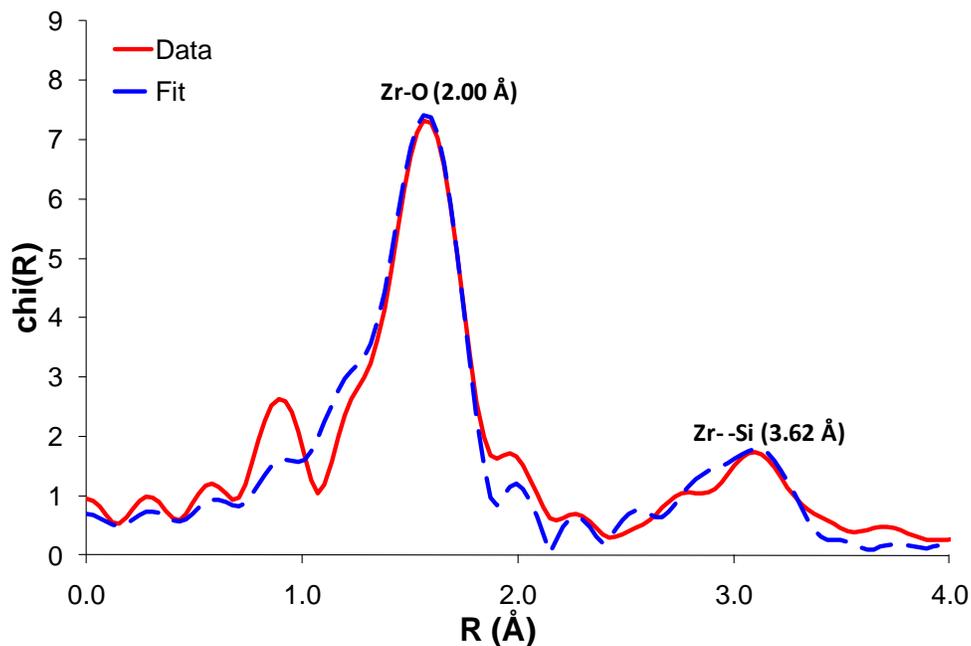


Figure 11: R-space plot first dose ZrCl₄

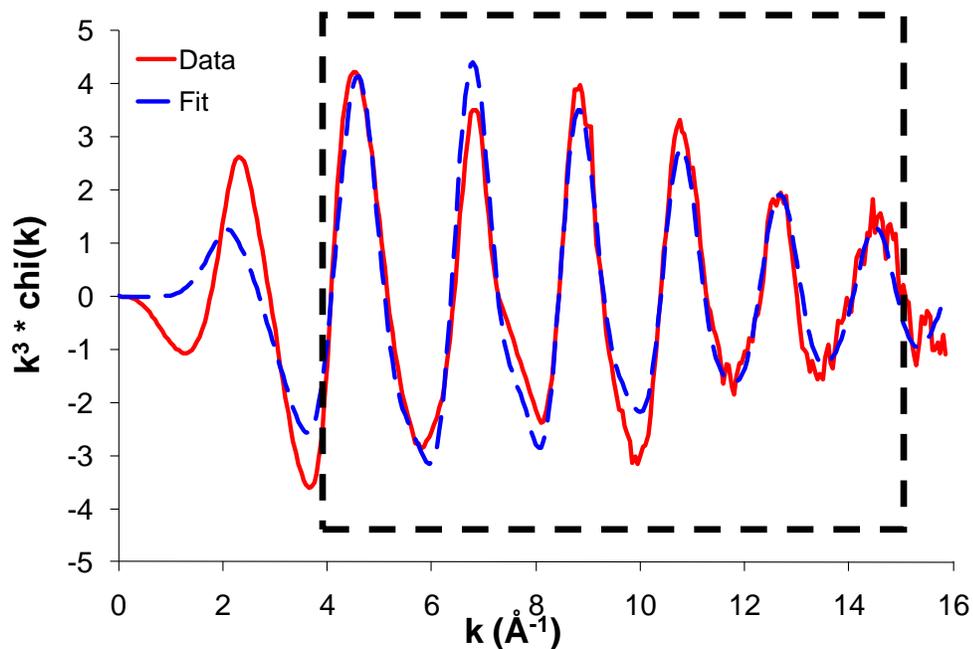


Figure 12: k-space plot first dose ZrCl₄

The gravimetric results of the second dosing step were consistent with the reaction of an average of two chlorides on each SiCl₄. The unreacted chlorides in the matrices may require passivation prior to studying the catalytic activity of these matrices. Similar fitting procedures were employed after the second dose of cross-linking ligand, SiCl₄ or SiCl₄py₂. Samples prepared with SiCl₄py₂ as the second chloride ligand differ from those prepared with SiCl₄ mainly in the surface area measured for the two samples. The surface area for the SiCl₄py₂ second dose samples is between one and two times larger than the surface area of the SiCl₄ samples. EXAFS data for SiCl₄ second dose samples were again fit to a tetrahedral structure around Zr with four Zr-O-Si bonds. The structural parameters, R and k-space plots for the Zr(OSi)₄ structural model can be seen in Table III, Figure 13, and Figure 14. The EXAFS data for the SiCl₄ second dose sample support the claim that the small oligomers present after the initial dosing step maintain the “embedded” nature of the zirconium centers after further cross-linking in a high surface area matrix. The fit data for SiCl₄py₂ as the second cross-linking reagent are

also summarized in Table III and the R- and k-space plots for this sample can be seen in Figure 15 and Figure 16. The EXAFS data for the SiCl₄py₂ second dose sample fit identically to the tetrahedral theoretical model used to fit both the first dose and SiCl₄ second dose samples. This suggests that pyridine does not bind to the zirconium centers in these silicate matrices when SiCl₄py₂ is used as the second dosing reagent.

Table III: Structural Parameters obtained from fits to second dose samples EXAFS data^a

	2 nd dose (SiCl ₄)		2 nd dose (SiCl ₄ py ₂)	
	Zr-O	Zr—Si	Zr-O	Zr—Si
R (Å)	1.98	3.61	2.01	3.66
σ ² (Å) ²	0.0036	0.0063	0.0042	0.0064
E ₀ (eV)	- 6.6 ± 1.9	E ₀ (O)	- 0.9 ± 2.0	E ₀ (O)
CN	3.6 ± 0.2	CN (O)	4.0 ± 0.2	CN (O)

^a Additional fitting parameters as follows: amplitude reduction factor(S_0^2) 0.928 (SiCl₄ and SiCl₄py₂). Fit figures of merit: 2nd dose (SiCl₄): FT k region: 4.2-15.6 Å⁻¹; X² 7738; reduced X² 386; R-factor 0.076. Non-EXAFS feature removal k region: 7.20-7.90 Å⁻¹. 2nd dose (SiCl₄py₂): FT k region: 4.2-15.4 Å⁻¹; X² 1065; reduced X² 54; R-factor 0.079. Non-EXAFS feature removal k region: 7.35-7.82 Å⁻¹.

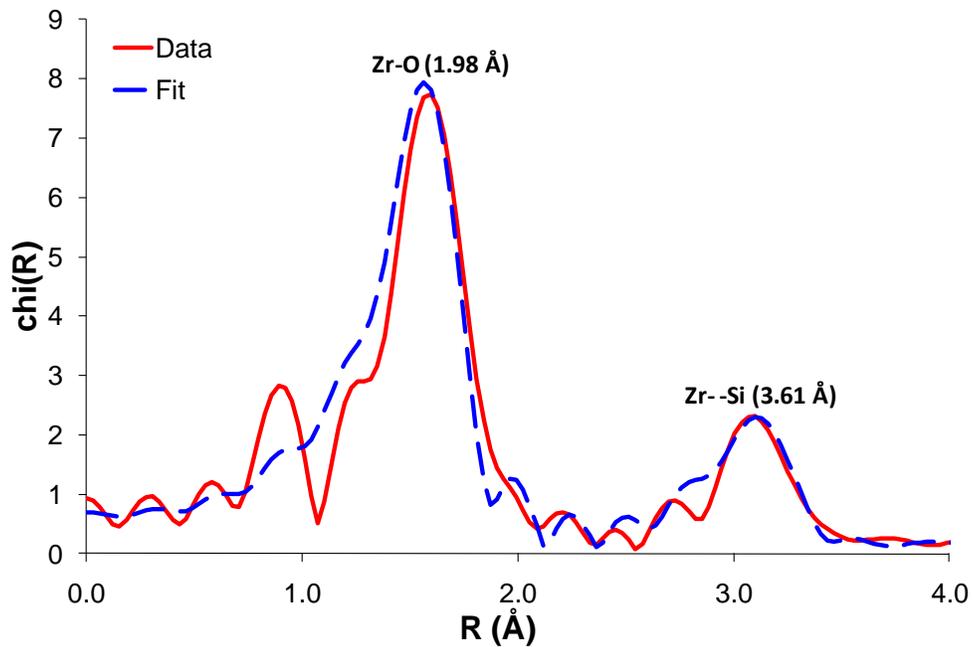


Figure 13: R-space plot second dose SiCl_4

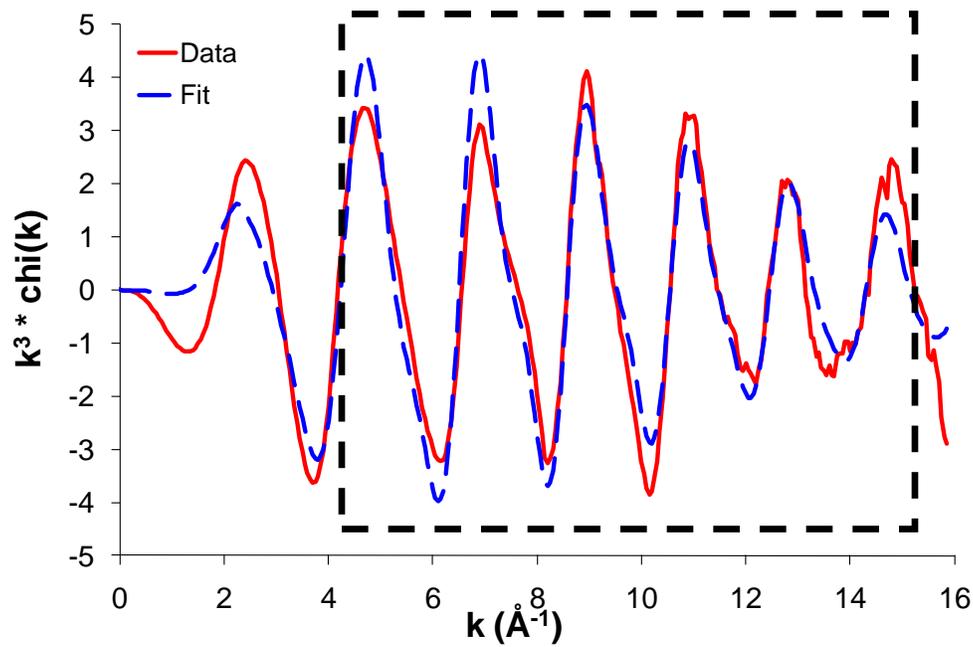


Figure 14: k-space plot second dose SiCl_4

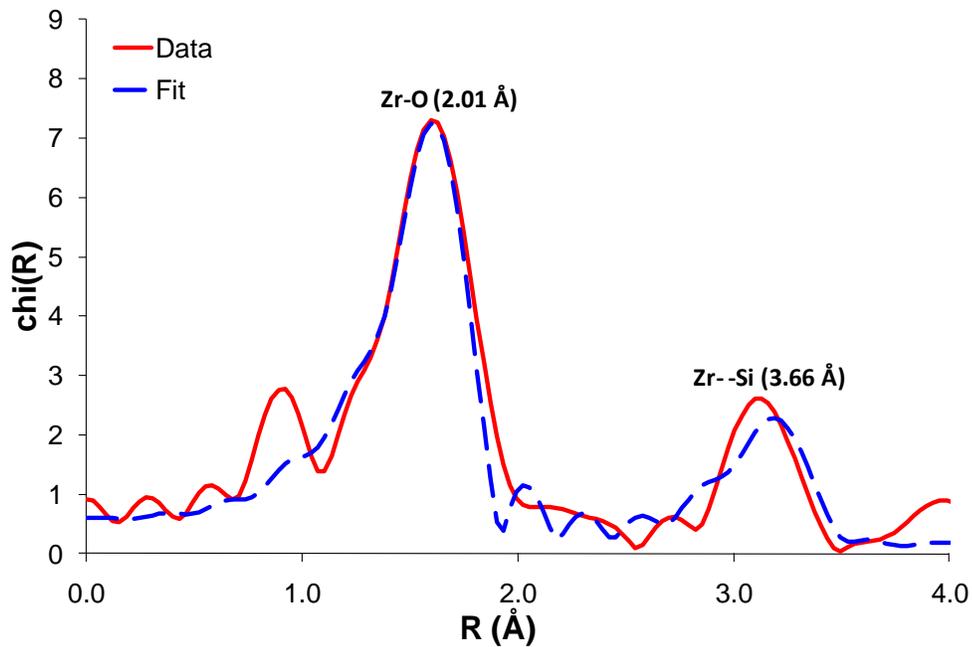


Figure 15: R-space plot second dose SiCl_4py_2

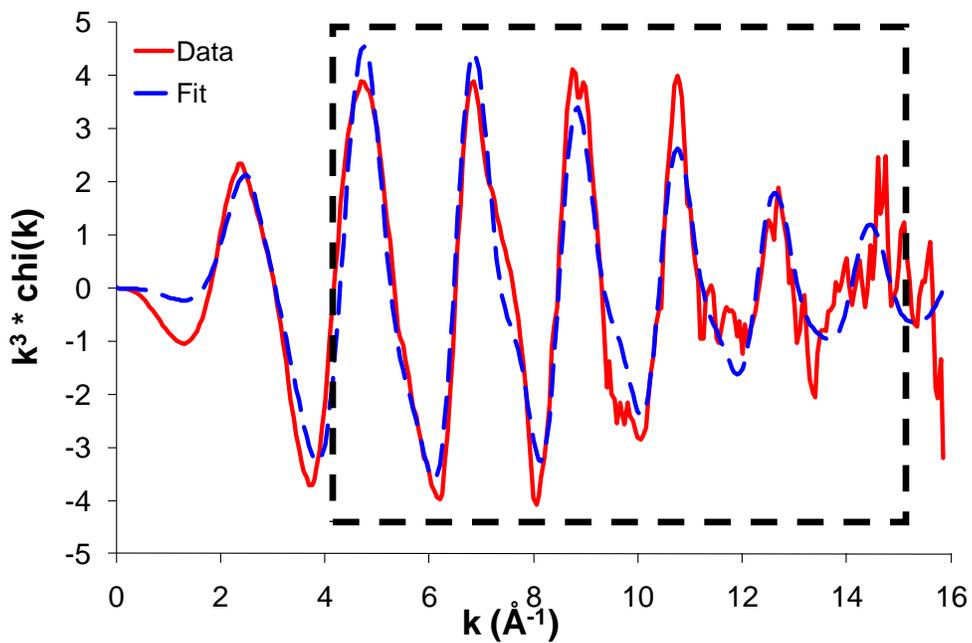


Figure 16: k-space plot second dose SiCl_4py_2

Pyridine binding to 4C-Zr: An IR Study

An IR spectrum of a sample with SiCl_4py_2 as the second chloride linking agent was taken to determine if pyridine was bound to the zirconium center, which was not seen in the EXAFS analysis. An excerpt of the spectrum shown in Figure 17 indicates pyridine is present in the matrix and is bound to the zirconium centers.

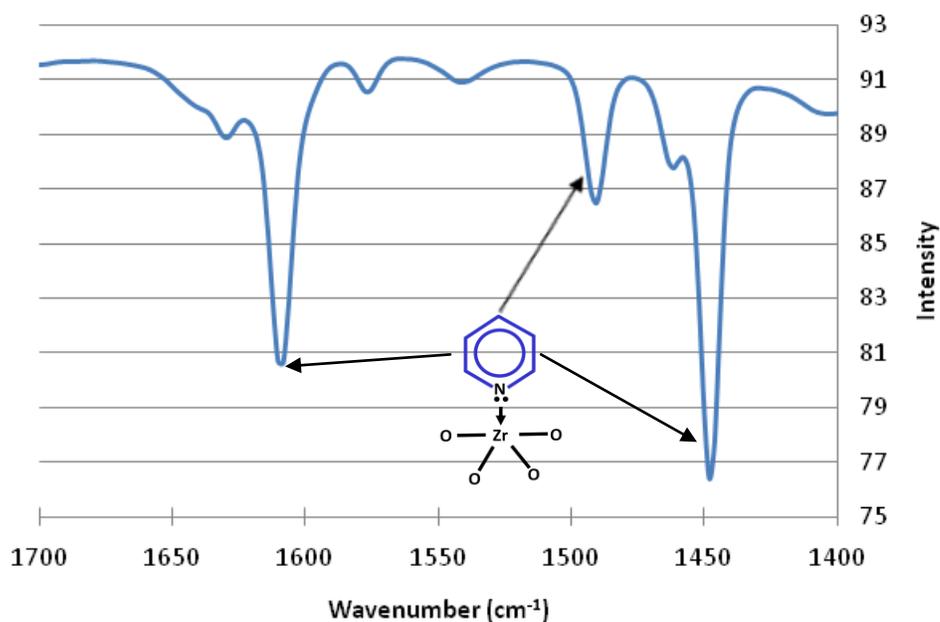


Figure 17: Excerpt of IR Spectrum showing C-C ring vibrations indicative of pyridine bound to Lewis acidic Zr sites

This discrepancy between the IR and EXAFS data may indicate that not all of the Zr centers within the matrix have bound pyridine. Having a majority of Zr centers without bound pyridine would result in the EXAFS data not predicting a structure with pyridine bound to zirconium. A method to quantify the number of zirconium centers with pyridine bound was developed based on Beer's Law. Preliminary results of analysis of second dose SiCl_4py_2 samples, after heating the sample to 100°C

under vacuum, indicate that 20% of the Zr sites have bound pyridine. Gravimetric and IR analysis of samples that were not heated revealed that each zirconium center had one bound pyridine.

Furthermore, the IR spectrum can reveal the acidic nature of the zirconium center based on the results of probing the centers with pyridine. These matrices can be categorized as having silanol, Brønsted acidic, or Lewis acidic sites as seen in Figure 18.

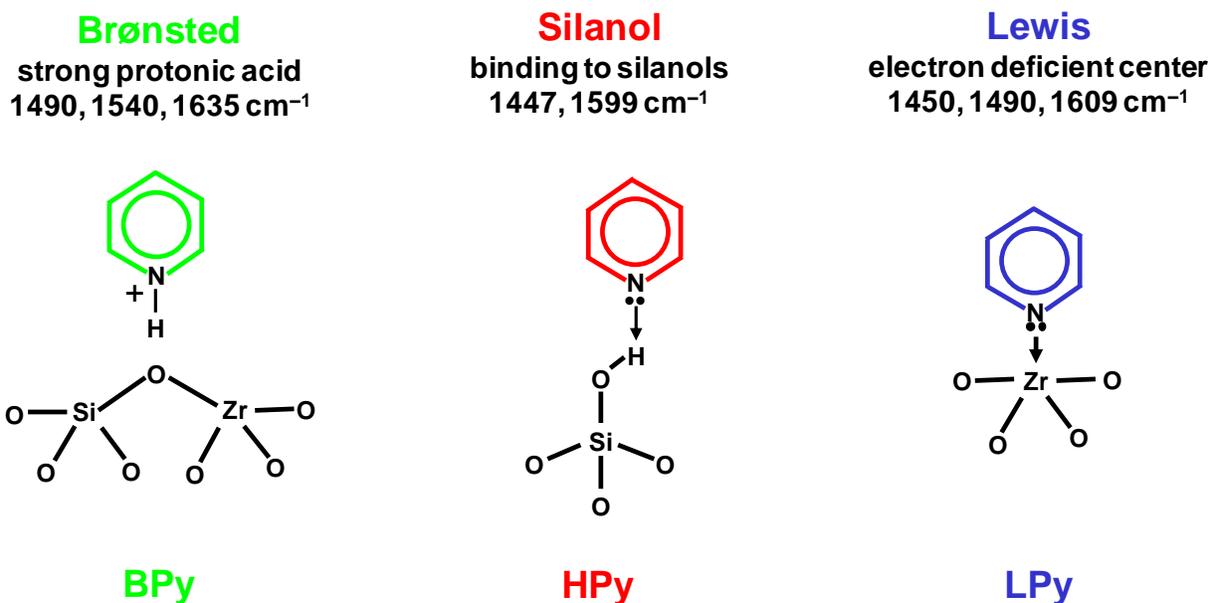


Figure 18: Potential acidic sites in the silicate matrices

These matrices should not have silanols because they are prepared in non-aqueous, non-protic environment. Thus, infrared spectroscopic analysis will mainly distinguish the zirconium centers as being either Brønsted or Lewis acidic in nature. The Lewis-acidity of the metal centers in these matrices is important to their catalytic capacities. Pyridine acts as a Lewis base in the donation of a lone pair present on the nitrogen and the zirconium centers accept these electrons making them Lewis acids. Based on the IR analysis the interaction between the pyridine and zirconium is a Lewis-acidic interaction. This conclusion was made from the presence of three peaks present in the IR

spectrum that characterize Lewis-acidic interactions at 1448 cm^{-1} , 1491 cm^{-1} , and 1608 cm^{-1} as seen in Figure 17.¹³

Surface Area versus Stoichiometric Dosing Ratios Study

To further understand the surface area and porosity of these materials, these properties were studied as a function of stoichiometry and dosing strategies described above. In an effort to tailor the surface area and pore size distribution of these matrices, several samples were prepared with varying stoichiometric ratios of linking reagent, SiCl_4py_2 , to $\text{Si}_8\text{O}_{20}(\text{OSnMe}_3)_8$ building block. Samples were prepared from a single dose of SiCl_4py_2 and the silicate building block. The surface area and pore size distribution were measured for each sample immediately after drying overnight at 100°C under vacuum. The observed trends for surface area versus stoichiometric ratio are summarized in Figure 19. In general, as the ratio of linker to cube is increased the surface area remains at zero up to a ratio of about 1:1, the surface area then increases rapidly until a ratio around 3:1, and then levels off at higher ratios. When the surface area plateaus there are no more small oligomers present in the system, but rather a high surface area, rigid matrix. Increased surface area makes the potentially catalytically active sites more accessible, which would lead to an increase in catalytic activity. The relationship between pore volume and stoichiometric ratios is very similar to that just described for surface area (Figure 20). Samples with a ratio of SiCl_4py_2 to tin cube of less than 1:1 are found to have no surface area and zero total pore volume. Furthermore, the maximum pore volume for these matrices corresponds to a stoichiometric ratio of 3:1.

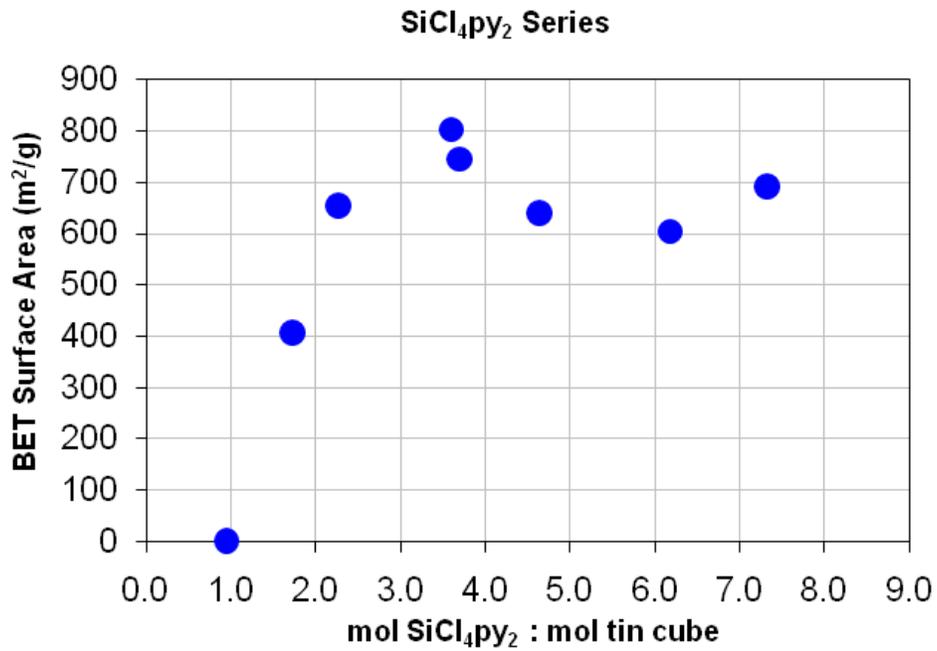


Figure 19: BET surface area versus stoichiometric ratio for a series of first dose Si materials

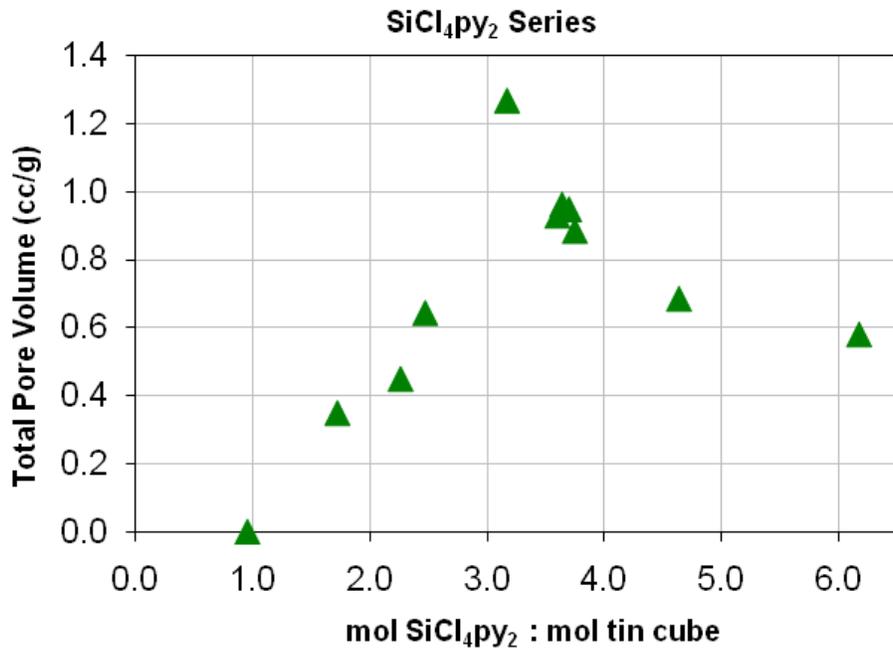


Figure 20: Total pore volume versus stoichiometric ratio for a series of first dose Si materials

The surface area for these silicate matrices is seen to increase rapidly as the stoichiometric ratio is increased and reaches a maximum of approximately 700-800 m²/g. The absorption and

desorption isotherms can further illustrate the different adsorption properties of the matrices for materials of low, less than 2.5:1, or high, 3:1 or above, stoichiometric ratios. Figure 21 displays the general shapes of the isotherms representative of both low and high stoichiometric ratio samples. The isotherm of a low stoichiometric ratio sample shows less of a rise in the volume of N₂ adsorbed, which is consistent with the lower surface area and pore volume measured for these matrices. In contrast, the isotherm of a high stoichiometric ratio sample has a more defined rise in the volume of N₂ adsorbed between a relative pressure of 0.4 to 0.8, which is also consistent with these materials possessing larger pore volumes. In Figure 22, the BJH plots comparing low and high stoichiometric ratio samples give further support of materials with increasing pore volume being produced at higher stoichiometric ratios. The well defined maximum of the BJH plot for a stoichiometric ratio of 3.75:1 corresponds to a pore radius of 50 Å, which is twice as large as the radius of approximately 25 Å for a smaller stoichiometric ratio of 1.72:1.

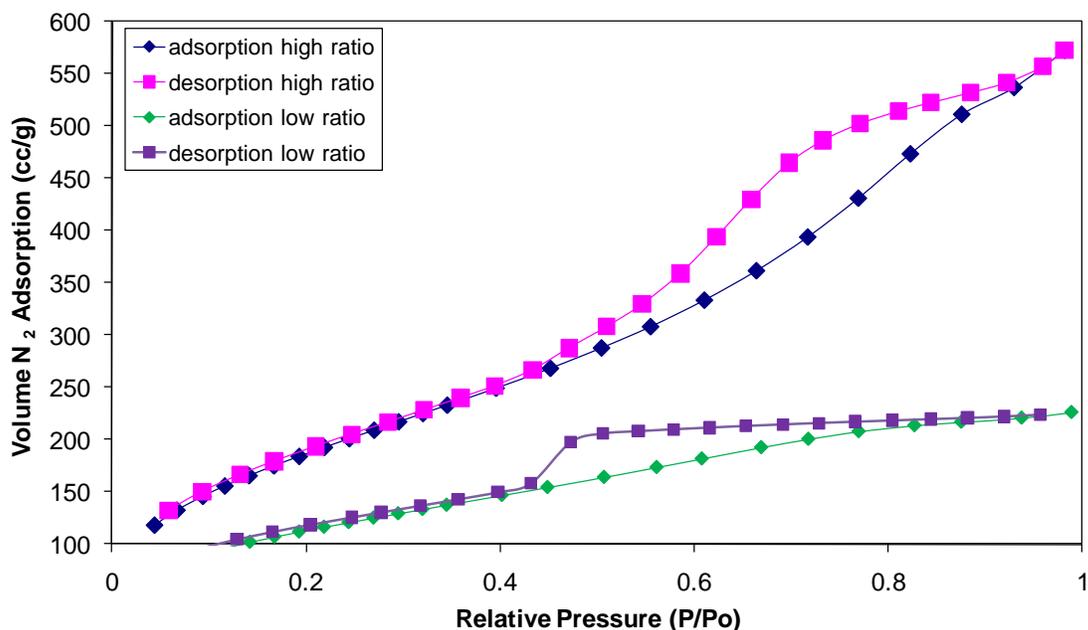


Figure 21: Comparison of adsorption and desorption isotherms for high and low stoichiometric ratios

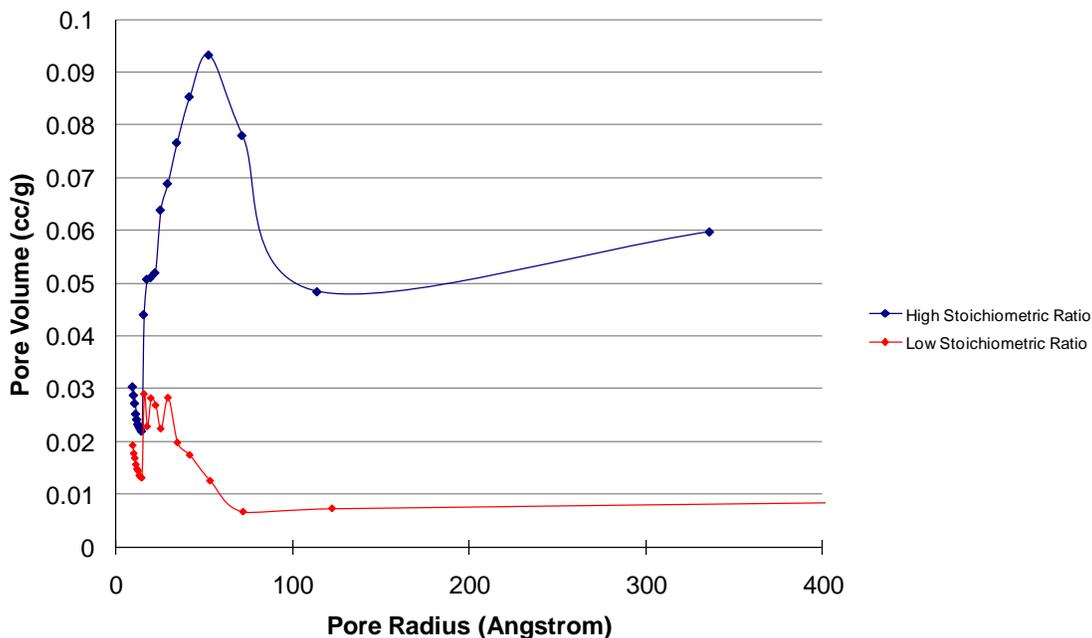


Figure 22: Comparison of BJH plots for high and low stoichiometric ratios

The results of this surface area and porosity study were applied to the methodology of synthesizing “embedded” titanium and zirconium centers in a high surface area silicate matrix. The stoichiometric ratio of catalytically active linking agent, $ZrCl_4$, to building block had to remain limiting at 0.5:1 as discussed previously, and a limiting amount of $TiCl_4$ at a ratio of 0.7:1 was used in a first dose step. These ratios produced consistent results with the 1:1 ratio of a $SiCl_4py_2$ first dose and possessed no porosity and had zero surface area. In the second dose step, the stoichiometric ratio of the cross-linking agent, $SiCl_4py_2$, could be altered in order to maximize surface area and pore volume for these matrices. The results of two second dose Ti samples and one Zr second dose sample reveal that the total stoichiometric dose, i.e. the sum of the mole equivalents for the first and second doses, leads to surface areas that are consistent with the curve seen in Figure 19. The results from these three samples have been added to the previous data for first dose $SiCl_4py_2$ samples as seen in Figure 23. A first dose $ZrCl_4$ sample at a ratio of 0.5:1 followed by a second dose of $SiCl_4py_2$ at a ratio of 3:1, which were the ratios mentioned previously that were used to produce

an embedded zirconium (IV) centers, was determined to be a high surface area material with a surface area of 881 m²/g.

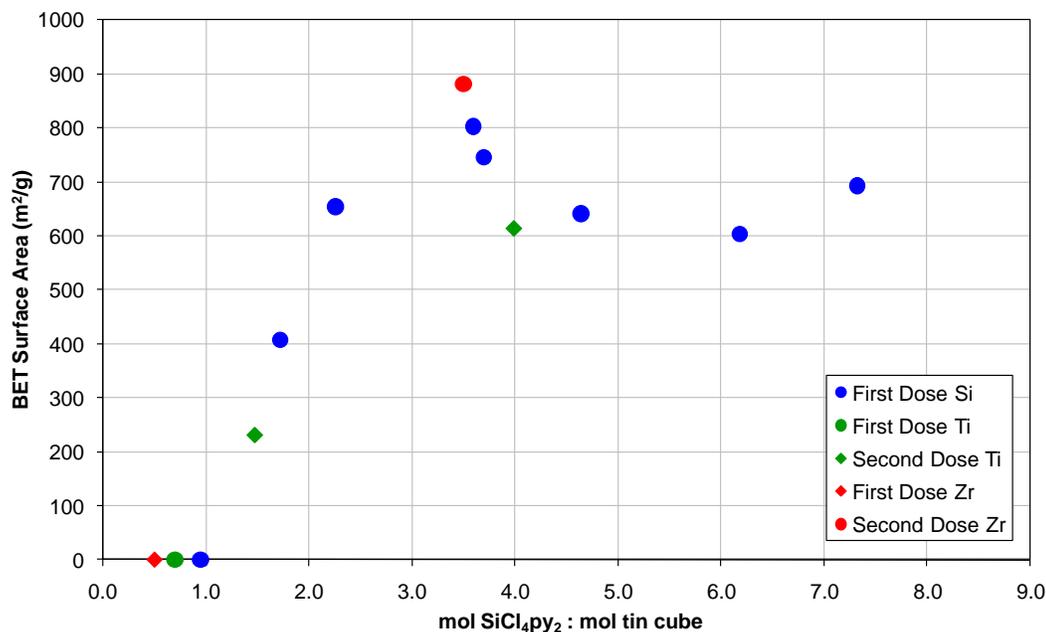


Figure 23: BET surface area versus stoichiometric ratio for a series of first and second dose Si, Ti, and Zr materials

Conclusions and Future Work

The synthetic procedures developed in this research form the basis of a new methodology for preparing silicate matrices with embedded, Lewis-acidic zirconium centers. These matrices were prepared using a method of sequential additions involving an initial transitional metal chloride, ZrCl₄, and second cross-linking chloride, SiCl₄ or SiCl₄py₂. Gravimetric and EXAFS analysis reveal the zirconium environment to be tetrahedral with four Zr-O-Si linkages after both the initial and second dosing steps. IR analysis confirms the Lewis acidic nature of the zirconium centers. An additional study of the relationship between stoichiometric ratio, linking reagent: building block,

and surface area allowed for the determination of conditions necessary to maximize the surface area of these zirconium silicate matrices.

The next step in the continuation of this project is the testing of the catalytic capacity of these matrices in various reactions. Furthermore, developing an appropriate method of passivation to remove any unreacted chlorides present after the second dosing step will also be a priority. There are several reports describing zirconium in silicate matrices as catalysts.^{8,9} These reactions include the epoxidation of ethylene to produce ethylene oxide and the oxidation of cyclohexane, cyclohexene, and vinyl-cyclohexene. Exploring reactions such as these in the presence of our single-site, heterogeneous catalyst will provide vital information about the relationship between the catalyst's structure and function.

Acknowledgements

We gratefully acknowledge the support of the U.S. Department of Energy-Office of Basic Energy Sciences, grant DE-FG02-01ER15259. Use of the National Synchrotron Light Source, Brookhaven National Laboratory, was supported by the U.S. Department of Energy, Office of Science, Office of Basic Energy Sciences, under Contract No. DE-AC02-98CH10886.

References

- (1) Schwarz, J. A.; Contescu, C.; Contescu, A. *Chemical Reviews* **1995**, *95*, 477.
- (2) Chu, C. T. W.; Chang, C. D. *The Journal of Physical Chemistry* **1985**, *89*, 1569.
- (3) O'Brien-Abraham, J.; Lin, Y. S. *Industrial and Engineering Chemistry Research* **2010**, *49*, 809.
- (4) Clark, J. C.; Saengkerdsub, S.; Eldridge, G. T.; Campana, C.; Barnes, C. E. *Journal of Organometallic Chemistry* **2006**, *691*, 3213.
- (5) Feher, F. J.; Weller, K. J. *Inorganic Chemistry* **1991**, *30*, 880.
- (6) Feher, F. J.; Weller, K. J. *Chemistry of Materials* **1994**, *6*, 7.
- (7) Lee, M.-Y.; Jiao, J.; Mayes, R.; Hagaman, E.; Barnes, C. E. *Catal. Today* **2011**, *160*, 153.
- (8) Dongare, M. K.; Singh, P.; Moghe, P. P.; Ratnasamy, P. *Zeolites* **1991**, *11*, 690.
- (9) Mehn, D.; Halasz, J.; Meretei, E.; Konya, Z.; Kiricsi, I. *Prague 2000, International Symposium & Exhibition on Environmental Contamination in Central & Eastern Europe, Proceedings* **2001**, 1937.
- (10) Piper, T. S.; Rochow, E. G. *Journal of the American Chemical Society* **1954**, *76*, 4318.
- (11) de Boer, J. H.; Lippens, B. C.; Linsen, B. G.; Broekhoff, J. C. P.; van den Heuvel, A.; Osinga, T. J. *Journal of Colloid and Interface Science* **1966**, *21*, 405.
- (12) Barrett, E. P.; Joyner, L. G.; Halenda, P. P. *Journal of the American Chemical Society* **1951**, *73*, 373.
- (13) Zhang, Y.-Q.; Wang, S.-J.; Wang, J.-W.; Lou, L.-L.; Zhang, C.; Liu, S. *Solid State Sciences* **2009**, *11*, 1412.
- (14) Ravel, B.; Newville, M. *Journal of Synchrotron Radiat.* **2005**, *12*, 537.
- (15) Newville, M. *Journal of Synchrotron Radiat.* **2001**, *8*, 322.
- (16) Zabinsky, S. I.; Rehr, J. J.; Aukudinov, A.; Albers, R. C.; Eller, M. J. *Physical Review B: Condensed Matter* **1995**, *52*, 2995.
- (17) Ankudinov, A. L.; Ravel, B.; Rehr, J. J.; Conradson, S. D. *Physical Review B: Condensed Matter* **1998**, *58*, 7565.
- (18) Clark, J. C.; Barnes, C. E. *Chemistry of Materials* **2007**, *19*, 3212.
- (19) Gaultois, M. W., Greedan, J. E., Grosvenor, A. P. *Journal of Electron Spectroscopy and Related Phenomena* **2010**, *In Press*.
- (20) Mountjoy, G.; Anderson, R.; Newport, R. J.; Smith, M. E. *Journal of Physics: Condensed Matter* **2000**, *12*, 3505.
- (21) Wang, W.-C.; Chen, Y. *Physica Status Solidi A Applications and Material Science* **1998**, *168*, 351.
- (22) Kawai, M.; Tsukada, M.; Tamaru, K. *Surface Science* **1981**, *111*, L716.